LONDON, METEOROLOGICAL OFFICE.
Met.O.19 Branch Memorandum No.96

The determination of broad band surface albedo
from AVHRR visible and near infrared radiances.

00691188 551.521.14 FH5B
551.507.362.2

MET O 19 BRANCH MEMORANDUM No. 96

The determination of broad band surface albedo from AVHRR visible and near infrared radiances

by

R.W. Saunders

August 1988

Meteorological Office Unit (Met O 19c)
Robert Hooke Institute for Co-operative Atmospheric Research
Clarendon Laboratory, Oxford, OX1 3PU

The determination of broad band surface albedo from AVHRR visible and near infrared radiances

Abstract

A method for retrieving broad band surface albedo from top of atmosphere reflected solar radiances measured by the visible and near infrared channels of the Advanced Very High Resolution Radiometer (AVHRR) is described. The algorithm developed was applied to eight passes over the British Isles and near Continent for relatively cloud-free conditions between the months of April and October. The retrieved surface albedos are presented both as high resolution images to show up the detail in the spatial variability and as tables where each value is an average over a 15 km grid square. The surface albedos of the agricultural areas of the British Isles showed a marked increase from 17 to 22% between April and July. In contrast urban areas and rougher hilly terrain (e.g. the Scottish Highlands) gave lower surface albedos of ~13% which remained more constant throughout the period between April and October. The results presented here are compared with those derived by other workers and found to be consistent with them bearing in mind the uncertainty of the method presented here which is about 4% in reflectance.

1. Introduction

One of the parameters required over the land surface for radiative transfer models is the reflectance of the surface, integrated over all visible and near infrared wavelengths and over all angles in the upward hemisphere. This quantity is known as the surface albedo which can be used to compute the magnitude of the reflected solar radiation at the surface, an important parameter for atmospheric radiative transfer calculations. The surface albedo varies with underlying surface type (e.g. coniferous forest, crops, urban development), snow cover, surface wetness and solar zenith angle. Surface albedo values are required for numerical weather prediction (NWP) models spatially averaged over each model grid square over land. For instance the mesoscale forecasting model developed by the U.K. Meteorological Office to cover the British Isles (Golding, 1984) currently assumes a surface albedo of 18% for all the grid squares containing land. It would obviously be desirable to replace this constant value with measured albedos which take into account the different surface types averaged over each grid square and the seasonal variations in albedo.

Satellite measurements have the advantage of uniform coverage with each value averaged over a well defined field of view. However a satellite views the surface through the atmosphere so the effect of the atmosphere on visible and near infrared solar radiation reflected at the surface has to be estimated which can introduce uncertainties in the retrieved surface albedo. Surface based or aircraft estimates of albedo are not ideal since unless they are taken over an area which is completely uniform the values actually measured will not be representative of a model grid square. Nevertheless they would be valuable for validating satellite estimates of surface albedo by identifying if there are any significant biases between them and the ground based measurements.

A recent comprehensive review of satellite measurements of surface albedo is given by Pinker (1985). There have been a number of methods already developed for deriving surface albedo from Meteosat visible radiances (e.g. Pinty and Ramond, 1987; Kriebel and Koepke, 1987; Dedieu *et. al.*, 1987), from GMS data (e.g. Nunez *et. al.*, 1987) and LANDSAT data (e.g. Brest and Goward, 1987). There have been a few papers on the retrieval of top of atmosphere albedo from the AVHRR (e.g. Wydick *et. al.*, 1987) for radiation budget studies and on the atmospheric correction for AVHRR visible channels (e.g. Singh and Cracknell, 1986; Kilsby, 1987), but to date a scheme specifically for retrieving surface albedo from AVHRR data has not been developed.

This paper describes a scheme to retrieve broad band surface albedos over the British Isles from visible and near infrared radiances measured by the Advanced Very High Resolution Radiometer (AVHRR) on the NOAA polar orbiting satellites. The scheme was applied to eight cloudfree passes of AVHRR data and the results are presented below.

2. Theory of the measurement of surface albedo

At visible and near infrared wavelengths there are three principal mechanisms which attenuate radiation as it passes through the atmosphere: molecular scattering (i.e. Rayleigh), aerosol scattering and gaseous absorption. The first two processes also scatter radiation into the beam increasing the radiance measured. Atmospheric emission at these wavelengths can be neglected. Figure 1 shows the various contributions to the measured radiance at the top of the atmosphere (TOA) for reflected and scattered solar radiation. To retrieve surface albedo from satellite radiance measurements these various atmospheric contributions have to be taken into account. Following Pinty and Ramond (1986) the filtered TOA radiance from a single channel, I_{TOA}, is given by:

$$I_{\mathrm{TOA}} = I_{\mathrm{SURF}}(z,\theta,\phi) + I_{\mathrm{RAY}}(z,\theta,\phi) + I_{\mathrm{AER}}(z,\theta,\phi) \tag{1}$$

where $I_{\mathrm{SURF}}(z,\theta,\phi)$ is the radiance reflected by the surface into the detector, $I_{\mathrm{RAY}}(z,\theta,\phi)$ is the Rayleigh scattered radiation, $I_{\mathrm{AER}}(z,\theta,\phi)$ is the aerosol scattered radiation, z is the solar zenith angle, θ the satellite zenith angle and ϕ the relative azimuth angle between the sun and satellite at the surface.

For most situations over land when z is less than 60° the surface radiance term dominates in equation (1). It can be expanded as follows:

$$I_{\mathrm{SURF}}(z,\theta,\phi) = I_S \cos(z) \Big[R_i(z,\theta,\phi)\tau_{\mathrm{tot}}(z)\tau_{\mathrm{tot}}(\theta) + r(z)R_i'(z)\tau_{\mathrm{tot}}'(z)\tau_{\mathrm{tot}}(\theta) + r(\theta)R_i(z,\theta,\phi)\tau_{\mathrm{tot}}(z)\tau_{\mathrm{tot}}'(\theta) \Big] \tag{2}$$

where $R_i(z,\theta,\phi)$ is the narrow band bidirectional surface reflectance averaged over the field of view for channel i, I_S is the filtered TOA equivalent solar radiance, $\tau_{\mathrm{tot}}(z)$ is the total atmospheric attenuation for the incoming solar radiation from the TOA to the surface and $\tau_{\mathrm{tot}}(\theta)$ is the attenuation from the surface to the satellite defined in more detail below. All the transmittances are integrated over the channel filter response. The first term on the right hand side of equation (2) is the directly reflected term which dominates. There are also contributions from downwelling diffusely scattered radiation which is then reflected directly into the beam as illustrated in figure 1 and also directly reflected radiation which is then diffusely scattered into the beam. These diffuse radiation contributions are included in (2) by the variable r which is the ratio of diffuse to directly transmitted radiation. The values for r were taken from the tables given by Braslau and Dave (1973). τ_{tot}' represents the transmittance for diffuse radiation and $R_i'(z)$ the surface hemispherical reflectance for downwelling diffuse radiation. Equation 2 neglects any second or higher order scattering terms for instance diffuse radiation scattered downwards, reflected by the surface and then scattered again in to the radiometer.

The total atmospheric direct transmittance $\tau_{\mathrm{tot}}(\zeta)$, for a zenith viewing angle ζ, can be split up into the following components,

$$\tau_{\mathrm{tot}}(\zeta) = \exp\left[-(\delta_{\mathrm{AER}} + \delta_{\mathrm{RAY}} + \delta_{\mathrm{GAS}})\sec(\zeta)\right] \tag{3}$$

where δ_{AER} is the mean aerosol optical depth, δ_{RAY} the Rayleigh optical depth and δ_{GAS} the mean optical depth due to gaseous absorption. The last term can be split up into three components, absorption due to water vapour, mixed gases and ozone. The total diffuse transmittance τ'_{tot} is assumed to have a total optical depth 20% higher than those assumed in equation 3 due to the longer path lengths through which the diffusely scattered radiation travels.

The Rayleigh scattered term, $I_{\mathrm{RAY}}(z,\theta,\phi)$, in equation 1 can be written as,

$$I_{\mathrm{RAY}}(z,\theta,\phi) = \frac{I_S \cos(z) P_{\mathrm{RAY}}(\psi)}{4(\cos(z)+\cos(\theta))}\left\{1 - e^{-\delta_{\mathrm{RAY}}(\sec(\theta)+\sec(z))}\right\}\tau_{oz}(z)\tau_{oz}(\theta) \tag{4}$$

where $P_{\mathrm{RAY}}(\psi)$ is the Rayleigh phase function for a scattering angle ψ which can be shown to be,

$$P_{\mathrm{RAY}}(\psi) = \frac{3}{4}(1+\cos^2(\psi)) \tag{5}$$

The scattering angle ψ can be computed from the solar and satellite zenith angles and relative azimuth angle by the following expression,

$$\psi = 180 - \cos^{-1}\left[\cos(\phi)\sin(\theta)\sin(z) + \cos(\theta)\cos(z)\right] \tag{6}$$

τ_{oz} is the atmospheric transmission due to ozone in the path which is primarily in the stratosphere above most of the molecules which cause the Rayleigh scattering. For more details on Rayleigh scattering theory the interested reader is referred to Tricker (1970).

The third term on the right hand side of equation (1) is the radiation scattered into the beam due to aerosols. This can be expanded as follows,

$$I_{\mathrm{AER}}(z,\theta,\phi) = \frac{I_S \cos(z) \tilde{\omega} P_{AER}(\psi)}{4(\cos(z)+\cos(\theta))}\left\{1 - e^{-\delta_{\mathrm{AER}}(\sec(\theta)+\sec(z))}\right\}\tau_a(z)\tau_a(\theta) \tag{7}$$

where $\tilde{\omega}$ is the aerosol single scattering albedo and $P_{\mathrm{AER}}(\psi)$ is the aerosol scattering phase function, both a function of aerosol type. τ_a is the atmospheric transmittance for aerosol scattered radiation given by,

$$\tau_a(\zeta) = \exp\left[-\left(\frac{\delta_{\mathrm{H2O}}}{2} + \delta_{mix} + \delta_{oz} + \delta_{\mathrm{RAY}}\right)\sec(\zeta)\right] \tag{8}$$

where δ_{H2O}, δ_{mix} and δ_{oz} are the optical depths due to water vapour, uniformly distributed gases and ozone respectively. The bulk of the aerosol scattering as depicted in figure 1 is assumed to be in the atmospheric boundary layer. Hence the scattered radiation will be attenuated by most of the gaseous absorption except water vapour which also mainly exists in the boundary layer. Therefore the assumption made here is that half the water vapour and all the mixed gases and ozone absorbs the scattered aerosol radiation.

Rearranging equation (2) and making the assumption that the surface hemispherical reflectance for diffuse radiation is the same as the bidirectional reflectance (i.e. $R'(z) =$

$R(z,\theta,\phi)$) we now get for the filtered bidirectional surface reflectance in channel i the following expression,

$$R_i(z,\theta,\phi) = \frac{I_{\mathrm{TOA}} - I_{\mathrm{RAY}}(z,\theta,\phi) - I_{\mathrm{AER}}(z,\theta,\phi)}{I_S \cos(z)\left[\tau_{\mathrm{tot}}(z)\tau_{\mathrm{tot}}(\theta) + r(z)\tau'_{\mathrm{tot}}(z)\tau_{\mathrm{tot}}(\theta) + r(\theta)\tau_{\mathrm{tot}}(z)\tau'_{\mathrm{tot}}(\theta)\right]} \tag{9}$$

We measure I_{TOA} for each channel and can estimate I_{RAY}, I_{AER}, τ_{tot}, τ'_{tot} and r, to obtain a value for $R_i(z,\theta,\phi)$.

To convert the filtered bidirectional reflectance to a broad band bidirectional reflectance, integrated over all wavelengths, the following is assumed. For a two channel radiometer at visible and near infrared wavelengths, as is the case for AVHRR, the broad band bidirectional reflectance $\rho(z,\theta,\phi)$ is given by,

$$\rho(z,\theta,\phi) = w_1 R_1(z,\theta,\phi) + w_2 R_2(z,\theta,\phi) \tag{10}$$

where R_1 and R_2 are the filtered bidirectional reflectances for each channel obtained using equation 9. w_1 and w_2 are the factors which weight each reflectance by the amount of incoming solar radiation in each channel. More exactly w_1, and w_2 are defined as,

$$w_1 = \frac{I_S(1)}{I_S} \qquad w_2 = \frac{I_S(2)}{I_S} \tag{11}$$

where I_S is the solar radiance integrated over all wavelengths, $\mathrm{I}_S(1)$ is the solar radiance integrated over all wavelengths less than the wavelength mid-way between the two channels (λm) and $\mathrm{I}_S(2)$ is the solar radiance integrated over all wavelengths greater than λm (i.e. $\mathrm{I}_S = \mathrm{I}_S(1) + \mathrm{I}_S(2)$).

Having obtained the bidirectional reflectance integrated over all wavelengths in a certain viewing direction (θ,ϕ) the surface albedo, $\rho(z)$, is determined by integrating the bidirectional reflectance over the upward hemisphere,

$$\rho(z) = \frac{1}{\pi}\int_0^{2\pi}\int_0^{\frac{\pi}{2}} \rho(z,\theta,\phi)\cos(\theta)\sin(\theta)d\theta d\phi \tag{12}$$

This can be approximated by using the following expression,

$$\rho(z) = \frac{\rho(z,\theta,\phi)}{f(z,\theta,\phi)} \tag{13}$$

where $f(z,\theta,\phi)$ are bidirectional reflectance factors which describe for a given surface type the variation of bidirectional reflectance with viewing angle.

The surface albedo, $\rho(z)$, is the parameter required for radiative transfer models as when multiplied by the incident solar flux it gives the upwelling reflected solar flux at the surface. The variation of $\rho(z)$ with solar zenith angle has been measured by the NIMBUS 7 ERB and is less than ten percent for land surfaces and solar zenith angles up to 60°

(Taylor and Stowe, 1984). The measured albedos can be normalised to a solar zenith angle of zero, ρ_0, using the expression,

$$\rho_0 = \rho(z)g(z) \tag{14}$$

where $g(z)$ is a factor derived from figure 8 of Taylor and Stowe (1984). This allows an albedo measured at one solar zenith angle to be converted into an albedo appropriate for a different solar zenith angle. The measured albedos, $\rho(z)$, reported below were only normalised using equation (14) when albedos for different passes were combined to compute a mean.

3. Application to AVHRR data

The scheme outlined in section 2 can be applied to TOA visible and near infrared radiances measured by the AVHRR which is an instrument on the NOAA polar orbiting satellites. Each satellite passes over the British Isles twice per day. The most suitable overpass for visible reflectance measurements is the afternoon pass at approximately 1430 GMT (which is currently the ascending pass for NOAA-9). At this time the solar elevation angle will be high enough for over half the year, over the British Isles, to make reasonable estimates of surface albedo. For solar elevations of less than 30° (i.e. from October to March), problems arise due to shadows on the surface, increased atmospheric contributions to the radiance, and greater departures from isotropic scattering (i.e. values of f well away from unity).

The AVHRR makes radiance measurements at 4 or 5 wavelengths (depending on the instrument) which are averaged over a field of view of 1.1 × 1.1 km^2 on the surface at the sub-satellite point. This area increases in size at the edges of the scan due to the viewing geometry. More details of the AVHRR are given in Kidwell (1985). For this study radiance data from the NOAA 9 visible (0.55–0.70 μm wavelength) and near infrared (0.71–0.98 μm) channels are used hereafter referred to as channels 1 and 2.

The data are received from the satellite as part of the High Resolution Picture Transmission (HRPT) data stream. Part of these data contain AVHRR channel 1 and 2 earth and space view counts which are then calibrated to give radiance in units of $W.m^{-2}.str^{-1}.\mu m^{-1}$. The AVHRR does not have an on board calibration target for the visible and near infrared wavelengths and so the calibration coefficients are determined in the laboratory before launch. They are then assumed to remain constant throughout the flight. A good review of the laboratory calibration of AVHRR channels 1 and 2 is given in Rao (1987). It has recently been found from post launch calibration of the AVHRR visible and near infrared channels from coincident aircraft measurements or simulated radiances that the gain α_i appears to have increased by about 15% for NOAA 7 after 2 years in orbit (Frouin and Gautier, 1987) and by up to 19% for NOAA 9 (Abel *et. al.*, 1988). This suggests that the sensitivity of these channels decreases gradually during flight.

The procedure used here is that employed in the APOLLO software (Saunders and Pescod, 1988) which is the one recommended by Price (1987). The raw counts C_i (or DN) in the HRPT data for channel i can be converted into radiance, I_i, using the expression:

$$I_i = \alpha_i C_i + \beta_i \qquad (W.m^{-2}.str^{-1}.\mu m^{-1}) \tag{15}$$

where α_i and β_i are the calibration coefficients in table 1 for NOAA 9 or for all satellites up to NOAA 10 in table 5 of Price (1987) and table 1 of Price (1988).

These radiances, I_i, are the filtered, TOA radiances in equations (1) and (9). In the APOLLO software these radiances are stored in the form of a Standard Image File (SIF) so that they can be quickly accessed and displayed. In order to reduce the number of calculations for each field of view (pixel) in the image, the solar and scattering angles are only computed once for every 32 × 32 pixel grid. Before the surface albedos are computed a cloud detection algorithm described by Saunders and Kriebel (1988) is applied to the radiance data to identify cloud contaminated pixels. The albedo of all cloud-free pixels are then computed assuming the viewing geometry at the centre of each 32 × 32 pixel array.

To derive the broad band surface albedo, $\rho(z)$, from the AVHRR radiances by the method described in section 2 a number of parameters integrated over the channel response functions have to be defined. Table 1 lists the values of these parameters assumed, for the results given in this paper, and their source. The absorption due to water vapour and mixed gases was calculated using a line by line transmittance model (Edwards, 1987). The computed transmittance due to water vapour for the standard midlatitude summer atmosphere over the wavelength range for NOAA 9 AVHRR channel 2 is shown in figure 2. The values for $P_{\mathrm{AER}}(\psi)$ and single scattering albedo, $\tilde{\omega}$, were derived from Mie calculations (Kilsby, 1988) applied to the continental aerosol model of Lenoble and Brogniez (1984) which produced the scattering phase functions for each channel shown in figure 3.

The weights, w_1 and w_2, to convert the filtered bidirectional reflectances to broad band reflectance used in equation 10, were computed for both channels using the shortwave model developed by Slingo and Schrecker (1982). The results suggested values of 0.5 for w_1 and w_2 assuming that $R_i(z, \theta, \phi)$ is constant in both channels. Note that the retrieved surface albedo is not very sensitive to the values of w_1 and w_2 assumed. A recent report by Wydick *et al.* (1987) gives regression coefficients for estimating TOA broad band albedos from TOA AVHRR filtered reflectances. However these coefficients cannot strictly be used here, for surface albedo, because of the different atmospheric attenuation in the two channels.

For the bidirectional reflectance factors, $f(z, \theta, \phi)$, used in equation 13, Koepke and Kriebel (1987) suggest using the values given by Taylor and Stowe (1984) rather than just assuming isotropy (i.e. $f = 1.0$ for all incident solar and satellite viewing angles). The problem with the Taylor and Stowe (1984) values is that they were derived from broad band TOA measurements and here they are applied to filtered surface radiances which have been combined to give a broad band radiance. If the bidirectional reflectance factors are wavelength dependent errors will be introduced. Also the factors used here are for all land types including desert which may not have the same angular behaviour as the vegetated surfaces over the British Isles. For this study results were computed both using the Taylor and Stowe (1984) reflectance factors and assuming isotropy. The albedo values were only normalised to a solar zenith angle of zero when albedos from different days were combined to compute a mean albedo. The values for $g(z)$ were also taken from Taylor and Stowe (1984).

The two parameters in table 1 which are the most variable are δ_{H2O}, which is proportional to the total column water amount, and δ_{AER} which is proportional to the amount of aerosols present in the path. Rather than use the climatological mean values for these parameters an attempt was made to use more representative values.

The water vapour optical depth, δ_{H2O}, for channel 2 was determined for a range of total column water amounts using the line by line transmittance model developed at Oxford (Edwards, 1987). This gave the following relationship between total column water amount, W (in kg/m^2), and computed water vapour optical depth integrated over the channel 2 filter response function,

$$\delta_{\mathrm{H2O}} = 0.102 \log_{10}(W) - 0.0346 \tag{16}$$

The constants are the best least square fit coefficients to the model results. W can be inferred from radiosonde ascents, humidity sounder retrievals (e.g. TOVS) or the difference between the brightness temperatures of the AVHRR infrared channels (4 and 5) over the sea. Any of these methods are only accurate to at best 10% in total water amount. For this study the mean difference between the AVHRR channel 4 and 5 brightness temperatures over the sea was used to provide a rough estimate for W using a regression relationship derived from simulated AVHRR brightness temperatures.

The value for δ_{AER} was estimated using the following procedure. Over the sea the bidirectional surface reflectance for channel 2, well away from areas of sunglint and suspended matter, can be assumed to be close to zero. Therefore to a first approximation equation (1) can be rearranged and written as,

$$I_{AER}(z,\theta,\phi) = I_2 - I_{RAY}(z,\theta,\phi) \tag{17}$$

where I_2 is the measured TOA channel 2 radiance and $I_{RAY}(z,\theta,\phi)$ is the computed Rayleigh contribution. Then, knowing $I_{AER}(z,\theta,\phi)$, δ_{AER} for channel i can be computed from equation (7). This will give an estimate of the channel 2 aerosol optical depth over the sea which is assumed here to be the same over the land. This may lead to an underestimate of the aerosol optical depth as there are normally higher aerosol concentrations over land. The value of δ_{AER} for channel 1 is then computed by multiplying the channel 2 value by the factor 1.36 to give the same ratio for δ_{AER} as for the default values listed in table 1. To compute values for $\rho(z)$, two passes must be made through the radiance data. The first pass computes $I_{AER}(z,\theta,\phi)$ for channel 2 using equation (17) for each 32×32 pixel array over the sea only on the side of the pass away from the sun. Effects such as undetected cloud, suspended matter on the sea surface or residual sunglint will all tend to increase the estimated value for $I_{AER}(z,\theta,\phi)$ so the minimum value is taken. The scattered radiance from this array is then assumed to originate only from atmospheric Rayleigh and aerosol scattering at channel 2 wavelengths so that equation (17) will be valid allowing a value for δ_{AER} to be computed. The second pass through the data then computes the surface albedo, $\rho(z)$, for each cloud-free pixel by using equations (9), (10) and (13), the parameters given in table 1, and the values for δ_{H2O} and δ_{AER} estimated as described above. Whilst it is realised that these two methods for estimating δ_{H2O} and δ_{AER} are not very accurate they are certainly better than assuming constant climatological values.

The resultant surface albedo images are then remapped from a space view projection to a polar stereographic projection as shown in the examples given in figure 4. These surface albedo plots are also averaged over the mesoscale model grid squares to produce a lower resolution dataset for NWP applications as tabulated in tables 4(a)–(h).

Before the scheme described above was applied to real AVHRR data a sensitivity study was carried out in order to ascertain how uncertainties in some of the values of the parameters assumed in table 1 affected the retrieved broad band surface albedo. The key parameters that were selected to investigate how uncertainties in their values affected the resultant albedo computed were α_i, δ_{AER}, δ_{H2O}, w_i, r and $f(z,\theta,\phi)$. These were varied by amounts which reflected their uncertainties. The results are shown in table 2. Measured count values of 106 and 230 were assumed for AVHRR channels 1 and 2 respectively and the satellite was at the zenith and the sun at a zenith angle of 35°. These are typical values over the British Isles for an early afternoon overpass of NOAA-9 during late June.

Table 2 shows that the parameters which have the biggest influence on the broad band albedo due to their uncertainty are the calibration coefficients for each channel α_i, δ_{AER}, δ_{H2O} and the bidirectional reflectance factors $f(z,\theta,\phi)$. The post launch values of α_i determined from ground based or aircraft measurements are only accurate to about 10% so this is currently an important limiting factor in obtaining more accurate surface albedos. This suggests that more effort should be taken in ensuring that satellite visible radiances are accurately calibrated after launch. As stated earlier there is some evidence that α_i increases by up to 19% after 2 years in orbit. All the results presented here assume the pre-launch calibration values given by Price (1988) for α_i. To roughly correct for the higher post launch values of α_i which have been reported, the albedos reported here should be increased by the percentage increase in α_i. Uncertainties in the anisotropic scattering of land surfaces will only be resolved by measurements from a satellite or aircraft radiometer which is able to view the surface from a variety of different viewing angles and for a wide range of solar zenith angles. Both aerosol scattering and water vapour absorption vary appreciably with airmass type (e.g. maritime – moist, continental – dry) and season. However changes of 50% in these parameters only altered the broad band surface albedo by 2% and as described above representative values for δ_{AER} and δ_{H2O} are used which should ensure the uncertainties for these two parameters are less than this. The retrieved surface albedo is also seen to be relatively insensitive to uncertainties in the weights w_i given to each channel or the diffuse/direct transmittance ratio r.

The results of this sensitivity study suggest that the broad band surface albedo can at least be measured to an accuracy of ±4% in albedo (all values of uncertainties quoted here are in *absolute* albedos, that is 4% in reflectance *not* 4% of ~ 20% reflectance). The relative changes in albedo within a single image can be measured to a much higher accuracy (~0.2%).

4. Results

A dataset of eight unusually cloudfree passes over the British Isles was obtained by searching through the University of Dundee archive of recent NOAA 9 afternoon passes. The passes were selected to test the retrieval algorithm for a range of different conditions and to determine if there was any seasonal variation in surface albedo. A list of the dates, viewing angles and also total column water amounts and channel 1 and 2 aerosol optical depths assumed is given in table 3. All passes were over the British Isles with small nadir viewing angles (i.e. $\sec(\theta) < 1.2$) except for the pass on 7 May 1987. The first pass (27 April 1984) was from NOAA 7, the remainder were from NOAA-9. With the exception of the calibration coefficients the parameters for NOAA 9, given in table 1, were used for all eight passes. As the differences between the filter response functions on both satellites are small there are no significant errors made in using NOAA 9 parameters with NOAA 7 data. Only the summer months were chosen (except for the 16 October 1986 pass) for this study to minimise problems due to low sun angles and long atmospheric paths which increase the uncertainties in the algorithm. The variability in retrieved total column water amount and aerosol optical depths is well shown in table 3.

The data from the eight passes were processed twice to obtain surface albedo, $\rho(z)$: once assuming isotropy (i.e. $f = 1.0$ for all angles in equation 13) and secondly using the values for f given by Taylor and Stowe (1984) (TS). For most cases the albedos computed using the second method were within 1% of those calculated assuming isotropy, as the TS values of f for small solar zenith angles ($< 45°$) and small satellite zenith angles ($<45°$) are close to one. The sun-satellite azimuth angles, ϕ, were in the range $0 - 35°$ and $180 - 215°$ for these passes. It was interesting to study the resultant differences in albedos computed for larger solar and satellite zenith angles. For the pass on 7 May 1987 which was the one case with relatively large satellite zenith angles ($\theta > 45°$) the application of the TS values gave more realistic albedos. For the case where f was assumed to be unity the surface albedos increased consistently across the track from west to east with increasing satellite viewing angle whereas the application of the TS factors produced more uniform surface albedos across the track. For cases with large solar zenith angles, such as the pass on 16 October 1986 ($z > 65°$), the effect of the TS factors was not so beneficial. For solar zenith angles greater than 60° the TS factors are derived from a much smaller set of observations (less than 25 per angular bin) whereas for angles less than 53° there are usually well over 100 observations per angular bin. When the TS factors were applied to the data for this pass large discontinuities in the resultant surface albedo were obtained. This may be due to the TS factors for these large solar zenith angles not being so representative as for the smaller solar zenith angles. For this reason, for solar zenith angles greater than 60°, the bidirectional reflectance factors were assumed to be one. For solar zenith angles less than or equal to 60° the TS factors were used. All the results described below were computed using this criterion. This will obviously increase the errors associated with surface albedos computed for low sun angles as isotropy is assumed here which is clearly not a good assumption. Only the pass on the 16 October 1986 is significantly affected by this assumption for the results presented here.

The surface albedo images computed for four of the eight passes are shown in figures 4(a)–(d) and for all eight passes the values averaged over mesoscale model grid points are

tabulated in tables 4(a)–(h). The dark areas are those pixels which were identified as cloud contaminated and so no surface albedo value could be computed from them. The diagonal stripes across some of the images show the boundary between the use of one TS f value and another.

The first pass, for 27 April 1984, shown in figure 4(a) was exceptionally cloudfree and gives albedo values for most of the British Isles and near continent. At this time of year most of Britain and Ireland have albedos in the range 14–20% with parts of southern Ireland and south west England slightly higher in the range 20–24%. The values on the near continent were also generally in this higher range with one well defined region (e.g. the Champagne region in northern France) with albedos as high as 30%. The effect of changes in the TS factors from one viewing angle to another can be seen in this image resulting in sudden changes in albedo of a few percent. A few weeks later in early May (though for a different year), figure 4(b), the surface albedo over the British Isles has increased to be in the range 17–22% except for the Scottish Highlands and urban areas, due to the vegetation increasing the reflectance at the longer near infrared wavelengths. The major urban conurbations such as London, Birmingham and Manchester maintain a low surface albedo of 12–14%. The third pass for 28 June 1986, figure 4(c), shows that the surface albedo values have increased by a few percent to be in the range 20–28%, except over the Scottish Highlands and Norway. The pass for the 16 October 1986, figure 4(d), shows the surface albedo to have decreased slightly by a few percent but still above the values recorded in the April pass shown in figure 4(a). This could be expected for the large solar zenith angles at this time (i.e. $g(z) \sim 0.7$). Uncertainties for this pass are higher than for the others due to the longer atmospheric paths and the assumption of isotropic scattering.

The variability observed between passes will be due to both seasonal and much shorter term day to day changes. The latter variability in surface albedo may depend on recent past weather (e.g. the amount of rain which has fallen during the previous week). The seasonal changes in surface albedo will depend mainly on the annual cycle in vegetation growth during the year but absolute values will vary from year to year depending on the types of crop grown and the previous weather in that year.

The mean of seven of the eight passes (16 October 1986 pass was excluded) normalised to a solar zenith angle of zero, ρ_0, is shown in figure 5(a) and tabulated in table 5(a). The mean albedo image shows that complete coverage was obtained of the British Isles and near continent. The cities show up well as areas of lower albedo (~12%) as do the Scottish Highlands, parts of western Ireland and the area in the region of Thetford forest, East Anglia. Over the agricultural areas of England and Wales a mean albedo of 17–19% is typical during the summer months. On the near continent mean albedos were as high as 22–26% over certain agricultural areas in northern France.

The variability in albedo, measured here by subtracting the maximum from the minimum value is shown in figure 5(b) and table 5(b). It illustrates that the urban areas and highlands have a low variability (~2–4%) whereas the agricultural areas experience a variability of 6–10%. It is interesting to note that the area inland from Calais has a relatively low variability (~3%) even though the mean albedo values are relatively high

(~18%).

5. Discussion

There have been a few satellite measurements of broad band surface albedo by other authors which can be compared with the values reported here. Dedieu *et al.*, (1987) use Meteosat visible channel radiances to infer surface albedos over France. Their values for July 1979 over northern France compare well with the values reported here for 4 July 1987. A study estimating surface albedos over Tasmania from the GMS visible channel (Nunez *et al.*, 1987) report albedos of 20% for 'pastured farmland' similar to that in Britain. James (1988) reports aircraft measurements of surface albedo over the Somerset levels for 16 October 1986. The aircraft values of 21% compare favourably with coincident values of 21–24% computed from the AVHRR data over the same area as shown in figure 4(d). Henderson-Sellers (1980) reports albedos in the 0.6–0.7μm wavelength band over Great Britain. This cannot be easily converted to broad band albedo but the relative albedo changes show some of the same features as those reported here (e.g. lower surface albedos over Scotland). These comparisons at least show that the method reported here is retrieving surface albedos consistent with those measured by other workers bearing in mind the uncertainty of this method is 4% in reflectance.

The complete annual cycle in surface albedo over the British Isles is difficult to determine due to the low sun angles during the winter months which increase the uncertainties in the method. However the changes in albedos from April to October reported here do show that whereas a constant albedo may be a good assumption over the Scottish Highlands and large urban areas, this is not the case for vegetated areas (e.g. pasture land, crops). Over southern England and northern France increases of up to 10% in surface albedo were noted between April and July. This seasonal variability should be included in models which make use of surface albedo in their radiation scheme. The spatial variability in surface albedo, well shown in figure 5(a), also underlines the fact that a single constant value of surface albedo over the British Isles is not a good assumption.

6. Conclusions

A method to retrieve surface albedo from AVHRR channel 1 and 2 radiances, allowing for variable aerosol optical depths and water vapour absorption is described. The estimated uncertainty is $\pm$4% in surface albedo which is mainly due to uncertainties in the calibration coefficients for the AVHRR channels 1 and 2. The bidirectional reflectance factors of Taylor and Stowe (1984) were used out to solar zenith angles of 60° but beyond this they gave unrealistic results and so isotropic scattering had to be assumed. Although this scheme is not designed to measure aerosol optical depth or total column water amount, the rough values obtained for these quantities were reasonable and could be used in the surface albedo retrieval, rather than climatological values. The values for surface albedo obtained over the British Isles are consistent with those obtained by other workers. Over the highland regions of Scotland surface albedos remained at 13% from April to October but over southern England the albedo typically increased from 17% in April to 22% in July.

Although the passes chosen for this study were unusually cloudfree, to get maximum

coverage for each pass, the scheme described here could be applied to AVHRR data on a routine daily basis. This would enable true monthly means to be calculated with different areas being clear for different passes. This will become a possibility when HRPT data from AUTOSAT-2 becomes available within the U.K. Meteorological Office in the near future.

7. Acknowledgements

The initial impetus for this research was provided by Dr. B. Golding (Meteorological Office) who was interested in the possibility of obtaining an improved surface albedo dataset for the mesoscale model from satellite data. I thank Dr. J. Foot and Mr. C. Kilsby of the Meteorological Research Flight, Farnborough for providing useful ideas and data for this project and commenting on this manuscript. The HRPT data was supplied by the University of Dundee satellite reception station.

8. References

Abel, P., Smith, G.R., Levin, R.H. and Jacobowitz, H. 1988 Results from aircraft measurements over White Sands, New Mexico, to calibrate the visible channels of spacecraft instruments. *Submitted to J. Geophys. Res.*

Braslau, N. and Dave, J.V. 1973 Effect of aerosols on the transfer of solar energy through realistic model atmospheres. Part I: Non absorbing aerosols. *J. Appl. Meteorol.* **12**, *601–615.*

Brest, C.L. and Goward, S.N. 1987 Deriving surface albedo from narrow band satellite data. *Int. J. Remote Sensing* **8** , *351–367.*

Dedieu, G., Deschamps, P.Y. and Kerr, Y.H. 1987 Satellite estimation of solar irradiance at the surface of the Earth and of surface albedo using a physical model applied to Meteosat data. *J. Clim. Appl. Meteorol.* **26** *79–87.*

Edwards, D.P. 1987 The new Oxford line by line atmospheric transmission/radiance model. *Memorandum 87.2, Dept. of Atmospheric, Oceanic and Planetary Physics.*

Frouin, R. and Gautier, C. 1987 Calibration of NOAA 7 AVHRR, GOES 5 and GOES 6 VISSR/VAS solar channels. *Remote Sensing of Environment* **22** *73–101.*

Golding, B.W. 1984 The Meteorological Office mesoscale model: its current status. *Meteorol. Mag.* **113**, *288–302.*

Henderson-Sellers, A. 1980 Albedo changes – surface surveillance from satellites. *Climatic Change* **2** *275–281.*

James, A. 1988 Remote sensing of seasonal variation in albedo over southern England. *Submitted as a PhD thesis, Dept of Geography, Nottingham University.*

Kidwell, K.B. 1985 NOAA polar orbiter data users guide. *NOAA/NESDIS/NCDC, Washington DC, 20233.*

Kilsby, C.G. 1987 The derivation of aerosol optical depth using AVHRR. *MRF internal note* **37**.

Kilsby, C.G. 1988 Private communication.

Koepke, P. and Kriebel, K.T. 1987 Improvements in the shortwave cloud-free radiation budget accuracy. Part I: Numerical study including surface anisotropy. *J. Clim. Appl. Meteorol.* **26** *374-395.*

Kriebel, K.T. and Koepke, P. 1987 Improvements in the shortwave cloud-free radiation budget accuracy. Part II: Experimental study including mixed surface albedos. *J. Clim. Appl. Meteorol.* **26** *396-409.*

Lenoble, J. and Brogniez, C. 1984 A comparative review of radiation aerosol models. *Beitr. zur Phys.* **57** *1-20.*

Neckel, H., and Labs, D. 1984 The solar radiation between 3300 and 12500 Å. *Solar Physics* **90**, *205-208.*

Nunez, M., Skirving, W.J. and Viney, N.R. 1987 A technique for estimating regional surface albedos using geostationary satellite data. *J. Climatology* **7** *1-11.*

Pinker, R.T. 1985 Determination of surface albedo from satellites. *Adv. Space Res.* **5** *333-343.*

Pinty, B. and Ramond, D. 1986 A simple bidirectional reflectance model for terrestrial surfaces. *J. Geophys. Res.* **91** *D7 7803-7808.*

Pinty, B. and Ramond, D. 1987 A method for the estimate of broadband directional surface albedo from a geostationary satellite. *J. Clim. Appl. Meteorol.* **26** *1709-1722.*

Price, J.C. 1987 Calibration of satellite radiometers and the comparison of vegetation indices. *Remote Sensing of Environment* **21**, *15-27.*

Price, J.C. 1988 An update on visible and near infrared calibration of satellite instruments. *Remote Sensing of Environment* **24**, *419-422.*

Rao, C.R.N. 1987 Prelaunch calibration of channels 1 and 2 of the AVHRR. *NOAA Tech. report NESDIS* **36.**

Saunders, R.W. and Pescod, R.W. 1988 A users guide to the A.P.O.L.L.O. scheme on HERMES/HOMER. *Meteorological Office internal report. Met.O.19 branch memorandum no.***87.**

Saunders, R.W. and K.T. Kriebel 1988 An improved method for detecting clear sky and cloudy radiances from AVHRR data. *Int. J. Remote Sensing* **9** *123-150.*

Singh, S.M. and Cracknell, A.P. 1986 The estimation of atmospheric effects for SPOT using AVHRR channel 1 data. *Int. J. Remote Sensing* **7** *361–377.*

Slingo, A. and Schrecker, H.M. 1982 On the shortwave radiative properties of stratiform water clouds. *Q. J. R. Meteorol. Soc.*, **108**, *407–426.*

Takashima, T. and Takayama, Y. 1986 Sea surface temperature measurement from space allowing for the effect of the stratospheric aerosols. *Papers in Meteorology and Geophysics* **37** *193–204.*

Taylor, V.R. and Stowe, L.L. 1984 Atlas of reflectance patterns for uniform earth and cloud surfaces (NIMBUS-7 ERB 61 days).*NOAA Tech. Rep. NESDIS* **10.**

Tricker, R.A.R. 1970 Introduction to meteorological optics. *Elsevier, New York.*

Wydick, J.E., Davis, P.A. and Gruber, A. 1987 Estimation of broadband planetary albedo from operational narrowband satellite measurements. *NOAA Tech. Rep. NESDIS* **27.**

Parameter*	Channel 1	Channel 2	Source
I_S	520 W/m^2/ster/μm	335 W/m^2/ster/μm	Neckel & Labs (1984)
α_i	0.523 W/m^2/ster/μm/DN	0.350 W/m^2/ster/μm/DN	Price (1988)
β_i	-18.9 W/m^2/ster/μm	-12.6 W/m^2/ster/μm	Price (1988)
δ_{H2O}	0.0 0.0	0.09 0.06	Typical values Mean UK July profile Mean UK Jan profile Line by Line model Edwards (1987)
δ_{mix}	0.0	0.023	Takashima & Takayama (1986)
δ_{oz}	0.032	0.0	Takashima & Takayama (1986)
δ_{RAY}	0.058	0.020	Kilsby (1987)
δ_{AER}	0.15	0.11	Typical values Takashima & Takayama (1986)
$\tilde{\omega}$	0.89	0.85	Kilsby (1988)
w_i	0.5	0.5	Slingo and Schrecker (1982)
$f(z,\theta,\phi)$	Table 2 of Taylor & Stowe (1984) 1.0	Table 2 of Taylor & Stowe (1984) 1.0	$z < 60°$ $z > 60°$
$P_{\mathrm{AER}}(\psi)$	see figure 3	see figure 3	Kilsby (1988)
$r_i(z)$	0.11–0.26	0.13–0.27	Braslau & Dave (1973)

* Notation as defined in section 2.

Table 1. Values assumed for NOAA 9 AVHRR channels 1 and 2.

	Channel 1 surface reflectance R_1	Channel 2 surface reflectance R_2	Broad band surface albedo $\rho(z)$
Ch1 count = 106 Ch2 count = 230	7%	32%	20%
	ΔR_1	ΔR_2	$\Delta\rho(z)$
Calibration coefficients α_i changed by 10%	2%	4%	3%
Aerosol optical depth δ_{AER} changed by 50%	1%	4%	2%
Water vapour optical depth δ_{H2O} changed by 50%	0%	4%	2%
Channel reflectance weights w_i changed by 10%	–	–	1%
Diffuse/Direct transmittance ratio r changed by 20%	0%	2%	1%
Anisotropic reflectance factor f changed by 10%	–	–	2%

Table 2. Sensitivity of retrieved surface albedo to input parameters. Solar zenith and azimuth angles are 35° and 230° respectively and the satellite is at the zenith. The values for ΔR_i and $\Delta\rho(z)$ are all in percent albedo not percentage error.

Time (GMT) and Date	$\sec(\theta)$	Total Column Water kg/m^2	Channel 1 δ_{AER}	Channel 2 δ_{AER}
1444 27 Apr 84	1.01	19	0.15	0.11
1347 21 Jun 86	1.04	16	0.12	0.09
1413 28 Jun 86	1.02	23	0.20	0.15
1429 19 Sep 86	1.09	21	0.07	0.05
1441 16 Oct 86	1.20	21	0.06	0.05
1420 23 Apr 87	1.01	23	0.15	0.11
1511 07 May 87	1.43	18	0.10	0.07
1449 04 Jul 87	1.06	26	0.09	0.07

Table 3. A list of AVHRR passes processed together with the total column water amount assumed and the aerosol optical depths inferred from the channel 2 minimum radiances.

SURF ALBEDO 23 APR 87 14:20Z

SURF ALBEDO 23 APR 87 14:20Z

Table 4(a) Surface albedo values for 23 April 1987 averaged over mesoscale model grid squares.

Table 4(b) Surface albedo values for 27 April 1984 averaged over mesoscale model grid squares.

Table 4(c) Surface albedo values for 7 May 1987 averaged over mesoscale model grid squares.

Table 4(d) Surface albedo values for 21 June 1986 averaged over mesoscale model grid squares.

Table 4(e) Surface albedo values for 28 June 1986 averaged over mesoscale model grid squares.

Table 4(f) Surface albedo values for 4 July 1987 averaged over mesoscale model grid squares.

Table 4(g) Surface albedo values for 19 September 1986 averaged over mesoscale model grid squares.

Table 4(h) Surface albedo values for 16 October 1986 averaged over mesoscale model grid squares.

ANNUAL MEAN SURFACE ALBEDO

ANNUAL MEAN SURFACE ALBEDO

Table 5(a) Mean surface albedo values of 7 passes (all but 16 October 1986) normalised to a solar zenith angle of zero averaged over mesoscale model grid squares.

Table 5(b) Maximum – Minimum surface albedo values for 7 passes (all but 16 October 1986) averaged over mesoscale model grid squares.

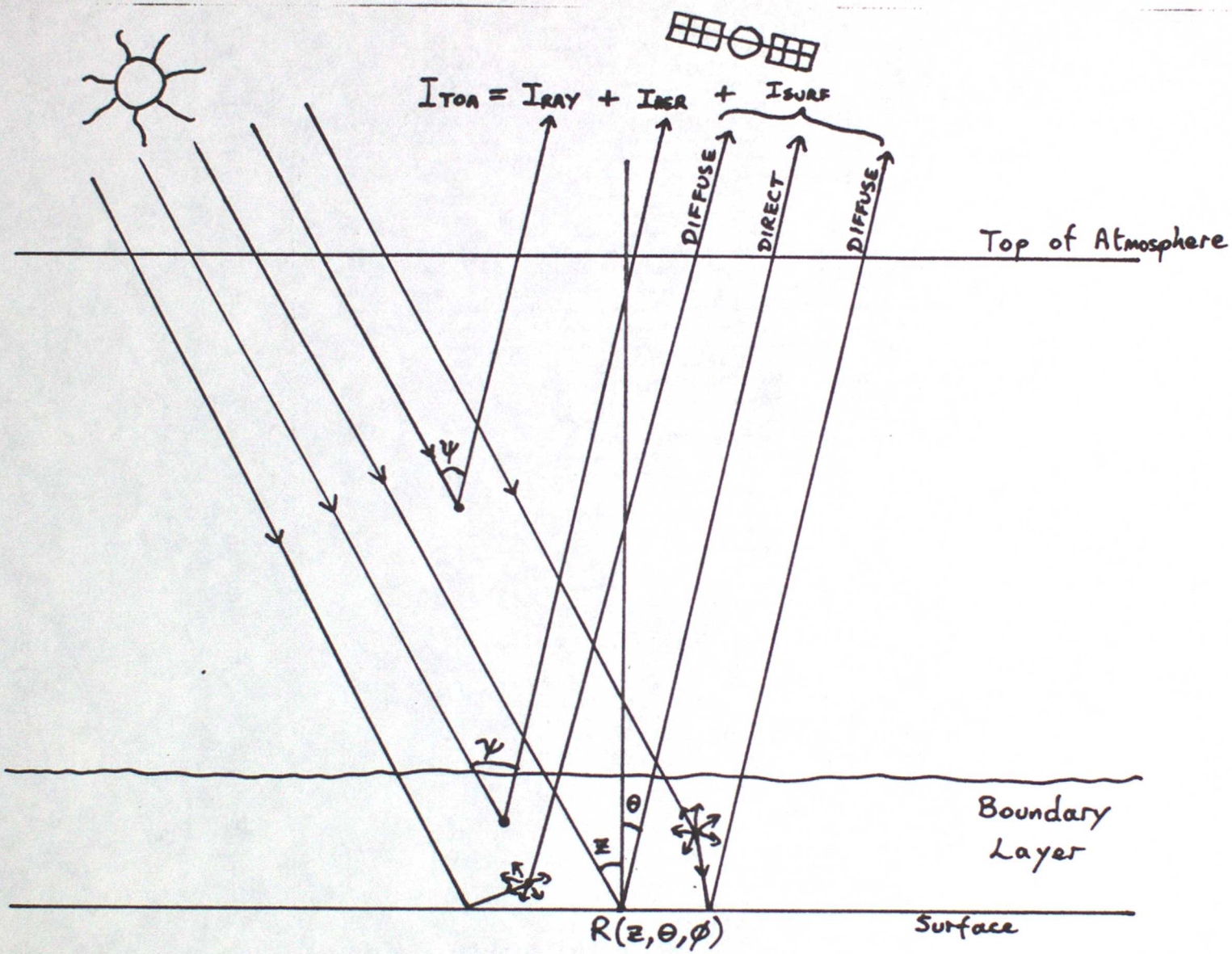

Figure 1. Diagram showing the different components of reflected and scattered radiation at visible and near infrared wavelengths.

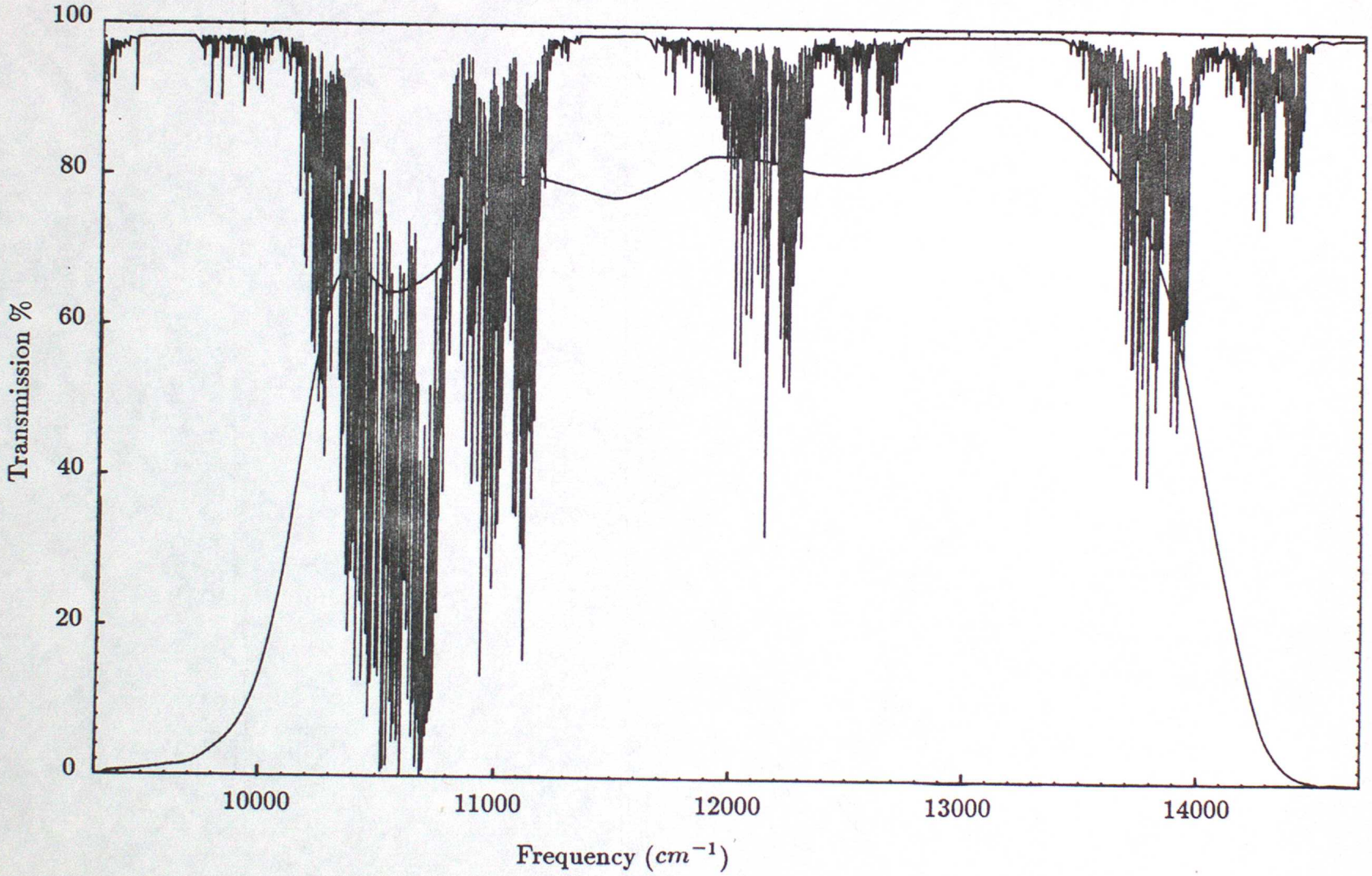

Figure 2. Atmospheric transmittance due to water vapour for a vertical atmospheric path from the surface to space for a standard midlatitude summer atmosphere (total column water amount of 29.3 kg/m^2) with the NOAA 9 channel 2 filter response function superimposed.

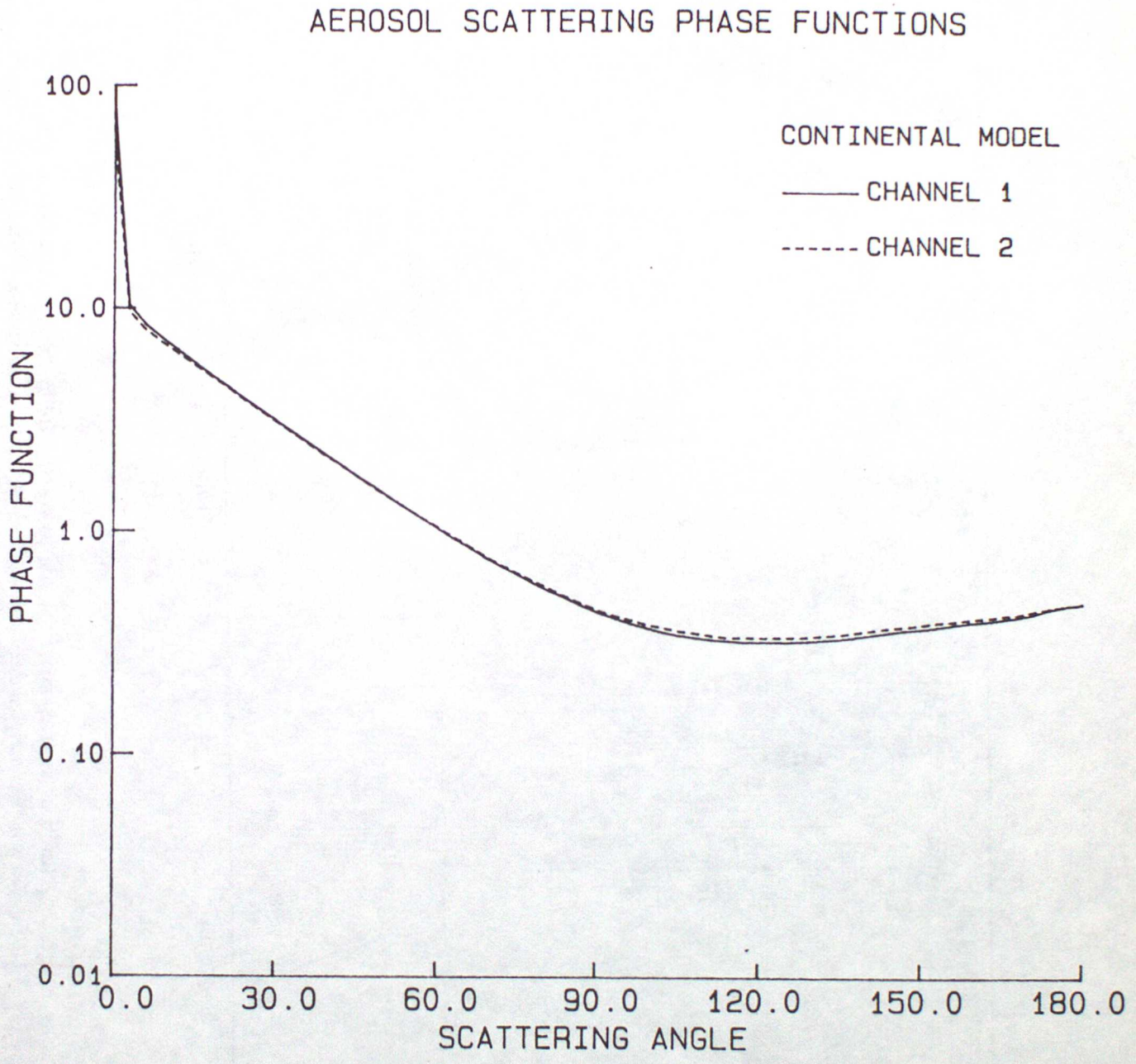

Figure 3. Normalised scattering phase function for continental aerosols. (after Kilsby (1988)).

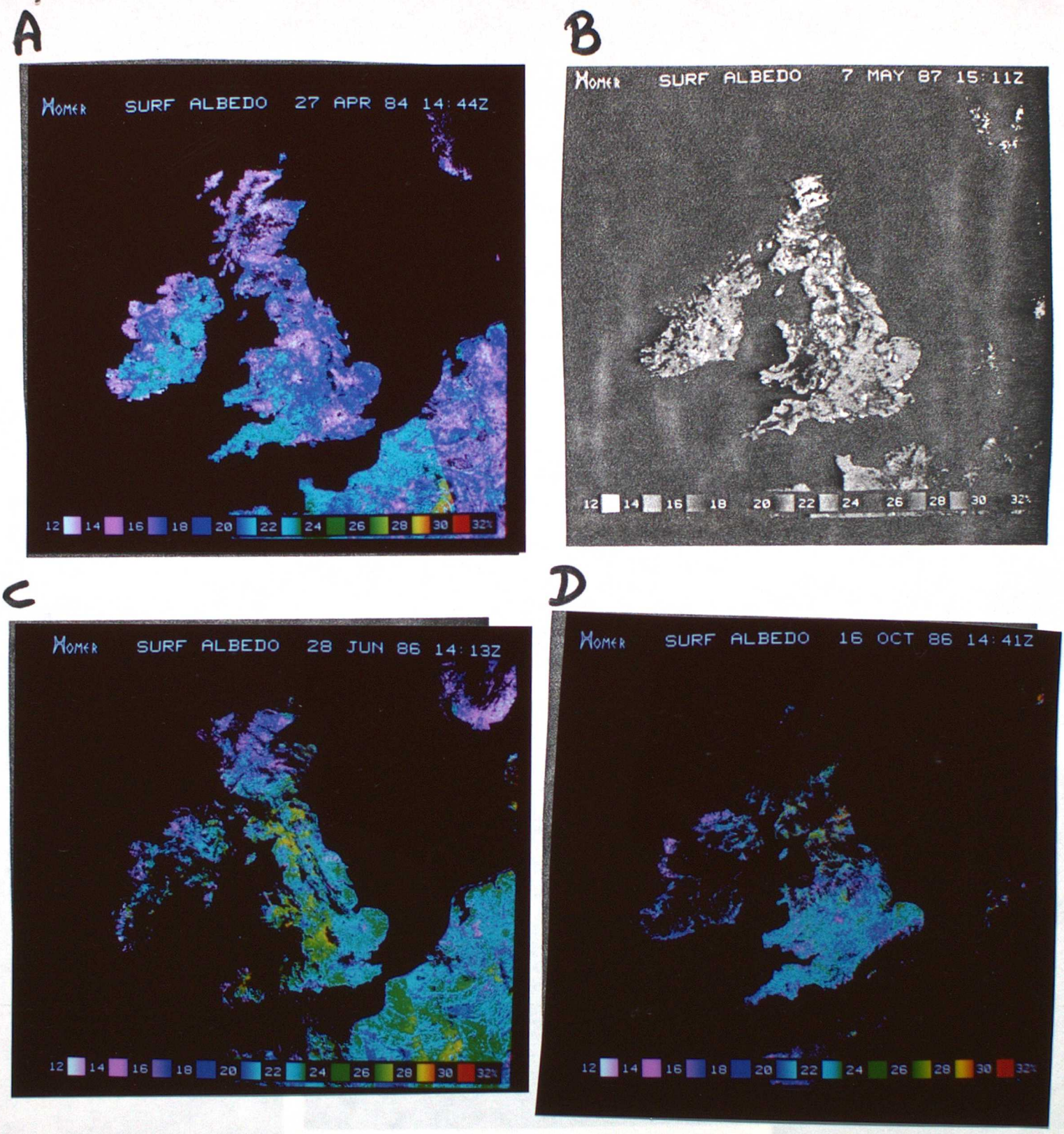

Figure 4. Images of retrieved surface albedo for (a) 27 April 1984, (b) 7 May 1987, (c) 28 June 1986, and (d) 16 October 1986.

A

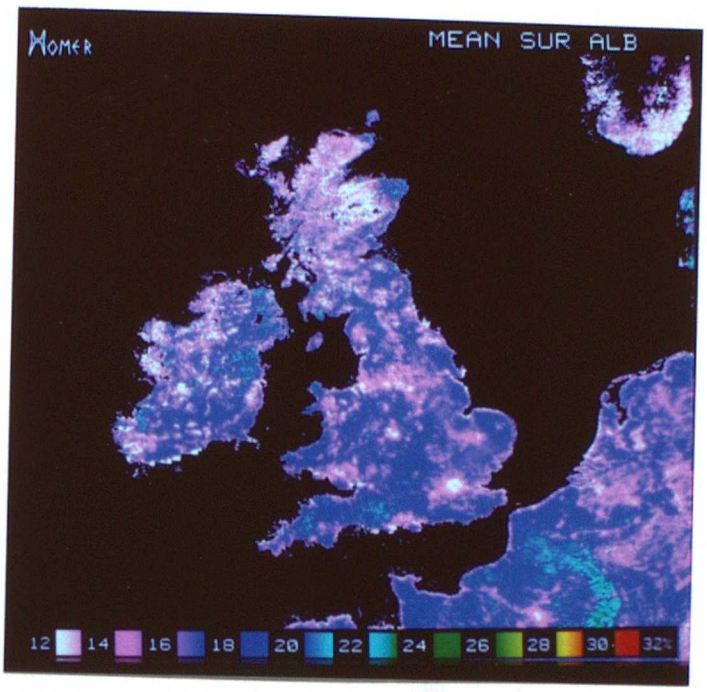

B

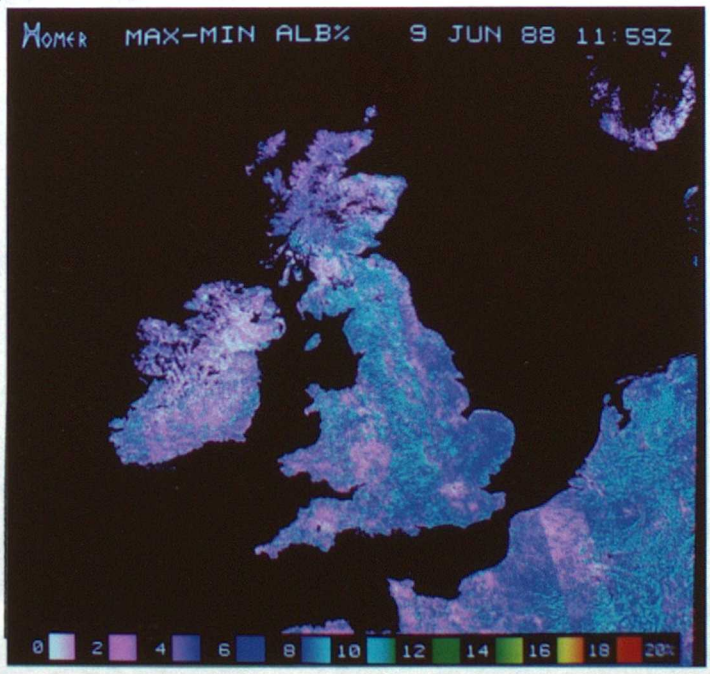

Figure 5(a) Average of retrieved surface albedo for seven passes (all except 16 Oct 1986) normalised to a solar zenith angle of zero and (b) the maximum minus minimum albedo for these seven passes.